Airborne test of a vector laser Doppler anemometer as true airspeed, angle of attack, and angle of sideslip sensor

Oliver Kliebisch[1], Peter Mahnke[1] and Matthias Damm[1]

1: Institute of Technical Physics, German Aerospace Center, Pfaffenwaldring 38-40, 70569 Stuttgart, Germany

Abstract: This study presents flight test results of a four-channel Laser Doppler Anemometer (LDA) for remote measurement of undisturbed airflow around an aircraft. The LDA system has been integrated into the DLR Falcon 20 research aircraft. Tests assessed LDA performance under varying atmospheric conditions and up to flight level 400. Initial findings on correlation, accuracy, and a statistical analysis of measurement rates and particle statistics are provided.

Keywords: Air Data Sensor, Lasers, Lidar, Laser Anemometer

1. Introduction

The primary parameters characterizing an aircraft's flight condition include true airspeed, angle of attack, angle of sideslip, barometric altitude, and air temperature. The Pitot-static system, temperature probes, and alpha/beta vanes are utilized to measure these parameters. Functioning as mechanical probes, these sensors indirectly measure the primary parameters within the boundary layer. Consequently, the sensors' performance is significantly affected by their mounting location and necessitates careful calibration to account for external influences.

Shortly after the invention of the laser, the potential for using lasers in flow velocimetry [1] and air data sensors [2] was recognized. This was motivated by the fact that active optical measurements of the relative wind vector could be performed outside of the boundary layer, and the measurement principle allows for the direct measurement of true airspeed and local airflow angles without measuring static/total air pressure [2-6]. A fuselage-flush mounting is possible, and dirt or icing on the optical window do not distort the measured values but instead result in increased and quantifiable measurement uncertainty. This property is sometimes referred to as "self-diagnostics."

In this paper, we present a four-channel laser Doppler anemometer (LDA) specifically developed for use as an optical air data sensor. The LDA technique relies on aerosol scattering in the Mie regime. Particles with a size on the order of the laser wavelength essentially move with the surrounding flow velocity. Narrow-linewidth laser light scattered by these particles exhibits a Doppler frequency shift in the radio-frequency domain, which can be detected using the principle of coherent detection. The frequency shift is directly proportional to the line-of-sight velocity of the particle. By measuring multiple distinct line-of-sight velocities, the full relative wind vector can be measured.

LDA has been tested in numerous flight campaigns over the last few decades; however, achieving the required accuracy and measurement rate under all flight conditions still poses significant technical challenges for an LDA system. Our system incorporates erbium-doped fiber laser technology and FPGA-based real-time processing. First, we will present the LDA system layout concerning both the optical layout and the digital signal processing scheme. Then, we will discuss the integration of the LDA instrument onto DLR's Dassault Falcon 20-E5 research aircraft and present results from two flight test campaigns conducted in 2022.

2. Laser Doppler flight test instrument

The developed LDA instrument for flight testing comprises two primary components: First, a flight rack that contains:

- A 3-unit LDA rack module described in section 2.1
- A 2-unit signal processing system described in section 2.2
- A 1-unit time server for synchronizing all timestamps to GPS time
- A 1-unit keyboard-video-mouse console for operating the system

The second primary component is an optical transceiver unit which is mounted in an optical port of the aircraft for sending/receiving laser light to/from the outside of the aircraft. This component is described in section 2.3.

2.1 LDA flight rack module

The 3U LDA module houses an in-house developed all-fiber laser Doppler anemometer, specifically designed for the flight test campaign requirements. Figure 1 illustrates the system layout schematically, while an image of the developed rack module is depicted in Figure 2. At the core of the system is an Erbium-doped fiber laser with a distributed feedback gain medium, achieving a linewidth of less than 15 kHz (NKT Photonics Koheras BasiK). The laser emits continuous-wave radiation at a 1550 nm wavelength, with an output power of 10 mW and an additional 1 mW in a monitor port, which serves as a homodyne local oscillator in the system. To enable

heterodyne detection, the main output is sent through an acousto-optic frequency shifter (AOF) operating at an 80 MHz shift frequency. The AOF's first-order shifted output is employed as a heterodyne local oscillator. A fiber-coupled switch, positioned just before the interferometer section's input, is used to switch between both local oscillators.

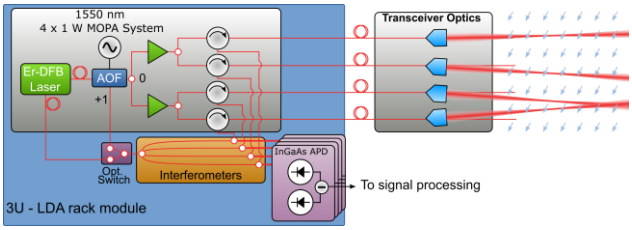

Figure 1: Schematic optical system layout of the four-channel laser Doppler anemometer.

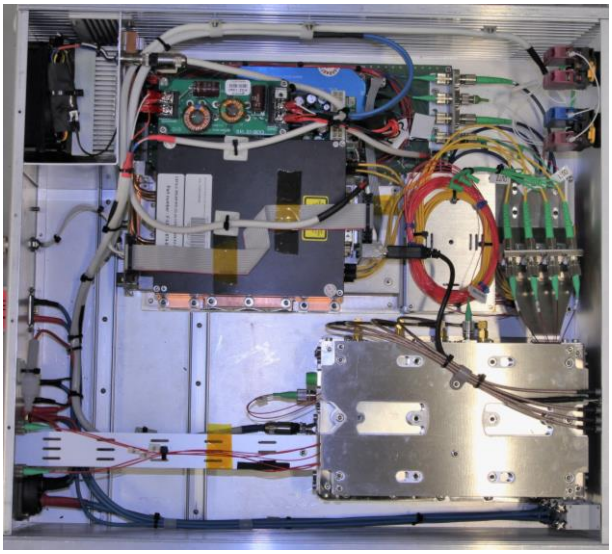

Figure 2: Image of the opened LDA rack module.

The AOF's zero-order port is split into two beams using a 50:50 fiber splitter and coupled into the input port of two erbium-doped fiber amplifiers (EDFA, NKT Koheras BoostiK). These EDFAs amplify the input light to an output power of 2 W. The output ports are internally divided into two ports per EDFA, yielding a total of four output ports with approximately 1 W of optical power each.

These four high-power ports are guided through fiber-optic circulators to employ a reference beam configuration. The circulator's purpose is to separate the transmitted beam from the received beam scattered by particles. The circulator output is guided via transfer fibers to four fiber imaging optics. Each fiber facet is imaged into the measurement volume at a slightly different angle, enabling vectorial flow measurement.

The detection and measurement of the line-of-sight Doppler shift are achieved by directing the backscattered light from the return port of all four circulators to a fiber-coupled interferometer/detector unit. The interferometer unit contains a 1x4 splitter, which evenly distributes the local oscillator (LO) power to all subsequent 2x2 splitters. The output fibers of the 2x2 splitters are connected to four balanced InGaAs avalanche photodiode (APD) receivers. The power supply, generating the APD bias high voltage, is housed within the interferometer unit, as well as a transimpedance amplifier for the photodiodes. The measurement bandwidth is approximately 150 MHz. Employing avalanche photodiodes ensures operation in the shot noise-limited regime over a wide range of local oscillator powers, starting at about 10 µW, at the expense of excess noise, which reduces the maximum signal-to-noise ratio (SNR).

2.2 MicroTCA based digital processing system

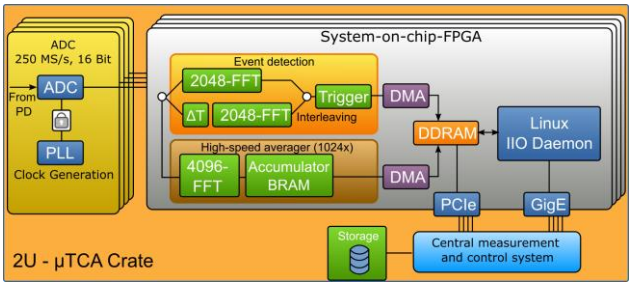

Figure 3: Schematic of the data processing scheme.

The photodetector signals are digitized and processed in real-time using a 2U MicroTCA computing system. Each photodetector signal is fed into an ADC FMC card connected to a Xilinx Zynq 7100 FPGA, which performs three parallel processing schemes.

The first and most crucial scheme is an event trigger, which continuously executes interleaved Fourier transforms of length 2048 (1st campaign) / 512 (2nd campaign), applies a frequency-dependent threshold function to the power spectrum, and sends detected particle spectra to the post-processing system (non-real-time). This scheme has proven highly sensitive in low aerosol environments for detecting weak signals buried in noise and robust against EMI (e.g., air traffic control radio) [7,8].

The second scheme is a spectrum average, where Fourier transforms of length 4096 are performed and averaged 1024 times before being continuously streamed to the post-processing system. This mode serves for diagnostics and system tests, working at higher scattering rates but not detecting very weak signals, as noise power accumulates while signal power reduces due to averaging.

To enhance real-time processing algorithms, a third mode is integrated, transmitting the raw photodiode signal via PCIe to the post-processing system and storing it directly on an attached SSD. Following improvements, this allowed us, during the 2nd campaign, to store all four channels at up to 2 GBytes/s with a duty cycle of typically over 90%. Due

to the large volume of data, this mode was used at the operator's discretion and did not record continuously. The raw data can be utilized to test improved algorithms or alternate parameterizations of our algorithms for further advancements in LDA technique.

2.3 Optical transceivers

As detailed in Section 2.1, the transmitted light is guided from the circulator through approximately 7 m long transfer fibers to the optical sensor plate. The sensor plate, with a diameter of 515 mm, is mounted in the designated viewport of the aircraft, as depicted in Figure 4.

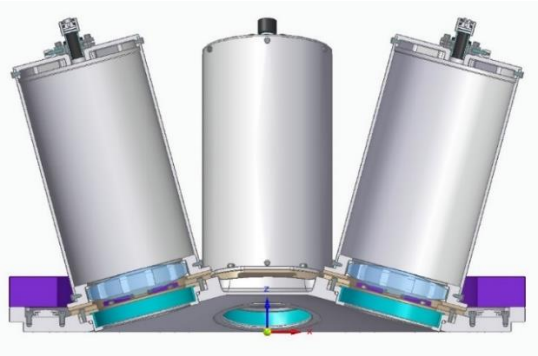

Figure 4: Cross-section through the optical sensor plate with 4 transceivers attached.

Four 100 mm fused silica windows, coated with a hardened anti-reflection coating for 1550 nm, serve as the optical interface between the cabin and the exterior of the aircraft. The windows are heated using eight positive temperature coefficient (PTC) heating elements mounted on the sensor plate, with a maximum heating power of 280 W. To enhance thermal contact between the aluminum sensor plate and the optical windows, thermally conductive silicone has been employed to secure the windows. This also assists in reducing mechanical stress on the windows during thermal excursions.

The LDA has been utilized with three different optical configurations, which can be altered by attaching various optomechanical subassemblies onto the window ports. All configurations share a 15° angle toward nadir, resulting in a non-zero Doppler shift for a perfectly level flight (at the improbable angle of attack of zero degrees).

The first configuration employs a commercial (Schäfter & Kirchhoff) fiber collimator with a 200 mm collimation focal length and a 500 mm singlet focusing lens. The second and third configurations utilize a custom-designed 4" aspheric lens, which images the fiber facet at measurement distances of 500 mm and 1000 mm, respectively. The aspheric lenses have been engineered to correct all spherical aberrations for this large aperture, demonstrating essentially diffraction-limited performance. The rationale behind these three configurations is to test the optimal LDA design to handle low aerosol environments at cruising altitude. A compromise must be struck between measurement volume and maximum signal strength. Increasing the aperture for a fixed measurement distance reduces the measurement volume but raises the minimum detectable aerosol size. For a volumetric scattering LDA, this compromise is balanced, and the signal-to-noise ratio (SNR) is almost independent of the aperture size [9,10], but in this case single scattering has to be considered.

3. Aircraft Integration

The flight test was conducted using the Dassault Falcon 20-E5 research aircraft, in service at DLR since 1976. This aircraft features several modifications to facilitate the integration of optical instruments, and in this case, the lower viewports were utilized. The ability to fly in similar cruise conditions as a typical airliner was an essential capability for these campaigns. For validation, the aircraft is equipped with a nose boom containing a five-hole probe, which extends from the nose and provides calibrated, accurate values for true airspeed, angle of attack, and angle of sideslip (among other parameters) at a 10 Hz data rate.

The instrument rack was positioned to the left of the aisle in the rear of the aircraft and connected to the 28 V supply power from the mission power bus, as shown in Figure 5. The transfer fibers were mounted within the cabin and routed over the ceiling to the LDA sensor plate. The sensor plate was installed in the front lower viewport, as depicted in Figure 6. The orientation was manually aligned, with best effort, to the aircraft's coordinate system, and any remaining deviations were calibrated/corrected during data evaluation. The sensor plate was secured by a ring and rubber sealings to ensure a pressure-tight fit.

Figure 5: LDA instrument rack

Figure 6: LDA sensor plate mounted in the front lower viewport with 4 apertures.

4. Flight test campaigns

Flight testing was conducted under a permit-to-fly during two campaigns, as shown in Figure 7. The initial 20-flight-hour campaign, carried out from Oberpfaffenhofen Airport, Germany (ICAO: EDMO), served as the instrument's preliminary test. Testing involved various flight conditions, including racetrack patterns, different ascent/descent rates, and flight levels up to FL400 within the TRA Allgäu. Although the instrument was permitted to operate starting at 1000 feet altitude, measurements commenced at higher altitudes due to a shutter door protecting the instrument during takeoff and landing.

At the end of each flight, a low-altitude pass by the lidar/ceilometer ground station at Hohenpeißenberg, operated by the German weather service, provided a reference for aerosol concentration in the boundary layer.

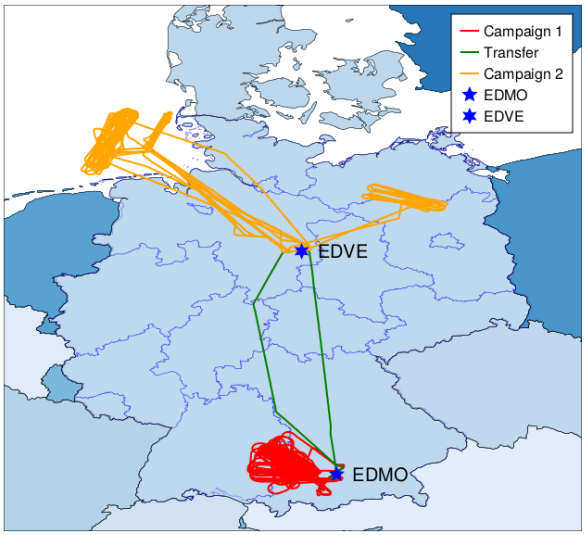

Figure 7: Overview of the flight tracks for the two flight test campaigns.

The second campaign was carried out from Braunschweig-Wolfsburg Airport (ICAO: EDVE), with 24 flight hours mainly focused on tracks over the North Sea to test the instrument's limits in low aerosol environments. This campaign also included more dynamic maneuvers, such as phugoid oscillations and 2 g full circles. The lidar ground station at Helgoland served as a reference for all but one flight during this campaign.

5. Results

The following results are based on event-trigger data, not raw data. For each detected particle event in each measurement channel during the flight, the timestamp and complex Fourier transform are saved. In post-processing, the steps outlined below are performed to determine the output values for TAS, AoA and AoS at a fixed rate of 10 Hz:

1. Perform a nonlinear least-squares fit of a Gaussian function to the measured LDA particle spectrum to obtain the Doppler shift frequency $\boldsymbol{f_{\mathbf{Doppler}}}$ and its uncertainty $\boldsymbol{\sigma_{f_{\mathbf{Doppler}}}}$.
2. Interpolate or decimate the Doppler shift frequency onto the noseboom's timestamp grid at 10 Hz for each channel.
3. Reconstruct the relative wind vector from individual channels using linear regression.
4. Apply calibration and correction for mounting angular errors and basic aerodynamic corrections:
    a. $\boldsymbol{\mathbf{TAS} = 1.02 \cdot \mathbf{TAS}_{\mathbf{RAW}}}$
    b. $\boldsymbol{\mathbf{AoA} = 1.5 \cdot \mathbf{AoA}_{\mathbf{RAW}}}$
    c. $\boldsymbol{\mathbf{AoS} = 0.7 \cdot \mathbf{AoS}_{\mathbf{RAW}}}$

The final correction step compensates for the non-optimal LDA mounting position several meters behind the aircraft's nose, causing the LDA to register rectified stream instead of free-stream flight angles. This phenomenological correction, which has not been validated by Computational Fluid Dynamics (CFD), works in most flight situations but has some limitations. Unoptimized compensation for mounting calibration is also evident as "cross-talk" between AoA and AoS. For a more application-ready system, a mounting position in the nose section of the fuselage should be used.

Figure 8 and 9 present measurement results from two representative flight days in each campaign, comparing them to the noseboom reference data in both time series and histograms of the residuals. The RMS deviation and standard deviation of the error distribution are provided. The first flight demonstrates the LDA's performance up to an altitude of FL400, while the second flight showcases its operation during more dynamic maneuvers. Steady-heading sideslip maneuvers were executed in both flights to test the LDA's calibration.

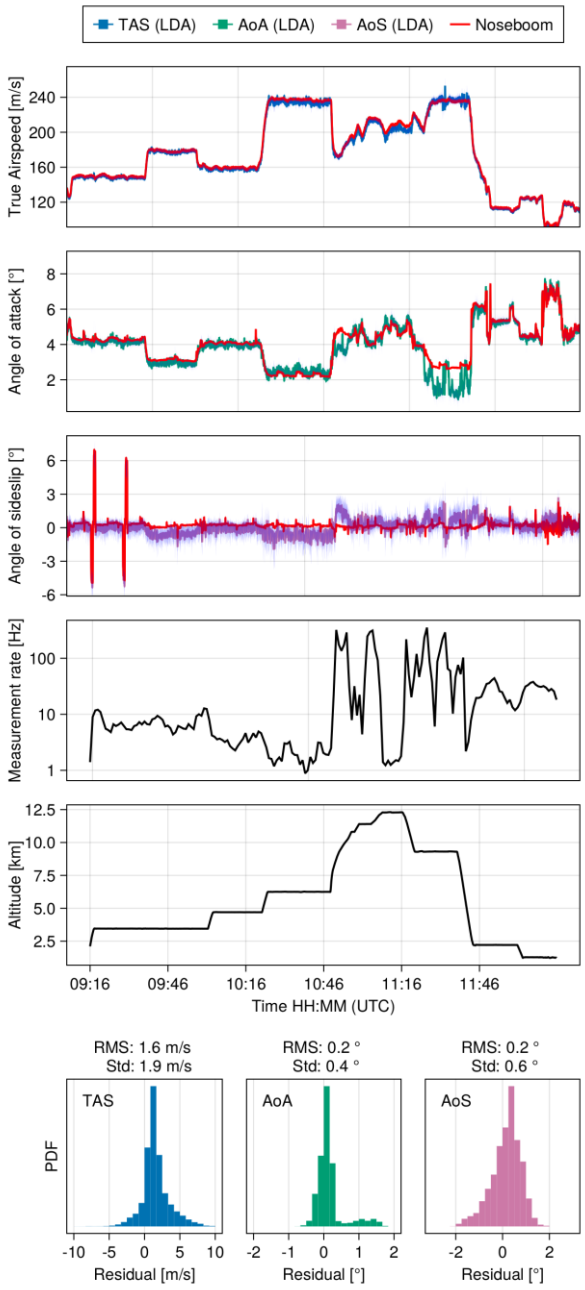

Figure 8: Results of flight day April 12, 2022.

The results indicate a good correlation between the instruments, although some deviations, particularly for AoA and AoS, can be observed in certain situations. These deviations are currently attributed to the oversimplified correction of aerodynamic effects resulting from the mounting position.

Compared to the noseboom, the LDA data exhibits higher noise levels. However, noise can be reduced by employing a Kalman Filter to combine the four individual LDA channels instead of using the interpolation approach, which causes computational noise/errors during vector reconstruction. This improvement is currently under development. In terms of measurement rates (combined for all channels), high variability is expected due to the abundance of aerosols as a highly variable atmospheric parameter. Measurement rates ranging from approximately less than 1 Hz to more than 100 Hz are observed for this signal processing scheme. Analysis of raw signals and detector sensitivity indicates that better signal processing and optimized detectors could potentially achieve at least an order of magnitude higher measurement rates.

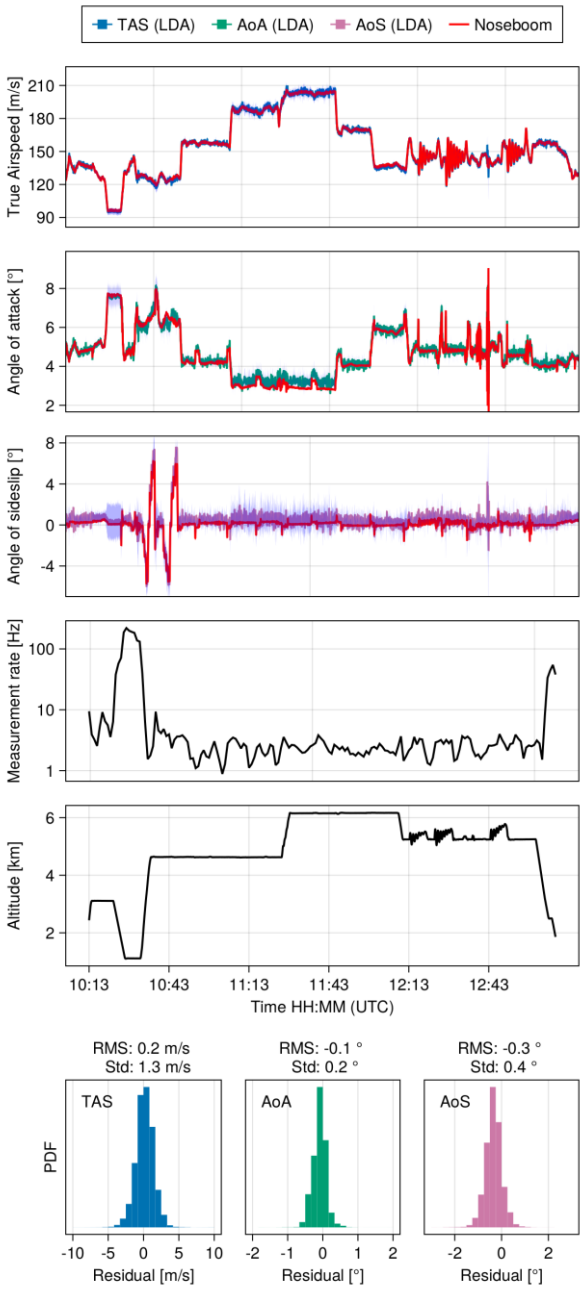

Figure 9: Results of flight day October 22, 2022.

5. Conclusion

We have presented flight test results of a four channel fiber-coupled reference beam laser Doppler anemometer. The system has been tested in-flight for more than 40 flight hours and was operational the full time. The results show a good correlation between a noseboom reference sensor and

the LDA values. Remaining inaccuracies can be reduced with a more systematic mounting of the LDA sensor plate as well as correction functions which consider the aerodynamic influences of the measurement location. Measurement rates between 1 Hz and more than 100 Hz have been encountered for different atmospheric conditions. Even in clear air conditions there was still a measurable signal, however the measurement rate was on the order of only 1 Hz.

There are several strategies for improvement of the measurement rate in clear air conditions. First, the real-time signal processing was not yet optimized and yields the easiest way for improvement. Second, the usage of APD-based photodetectors limits the SNR of the sensor and can be replaced by photodetectors for about a fivefold improvement of SNR. Third, the system was built using fiber connectors and not spliced and polarization optimized splices. There are further possibilities (e.g. increasing the laser power) which could be considered but might have detrimental effects on the size, weight and power of an LDA based optical air data sensor.

6. Acknowledgement

The authors acknowledge the contribution of their colleagues to this work.

6. References

[1] Y. Yeh and H. Z. Cummins: "*Localized Fluid Flow Measurements with an He-Ne Laser Spectrometer*", Applied Physical Letters, 4, 176-178 (1964).

[2] R. Muñoz, H. Mocker and L. Koehler: "*Airborne Laser Doppler Velocimeter*", Applied optics, 13 (12), 2890–2898, 1974.

[3] M. Verbeke: "*LIDAR Airborne Aerodynamic Sensors*", WAKENET-3 Europe/Greenwake Workshop (Palaiseau, France), 2010.

[4] M. Beversdorff, W. Förster, R. Schodl, and H. W. Jentink: "*In-flight Laser Anemometry for Aerodynamic Investigations on an Aircraft* ", Optics and Lasers in Engineering, 27 (6), 1997.

[5] H. W. Jentink, H. Kannemans, and M. J. Verbeek: "*In-Flight Evaluation of an Optical Standby Air Data System*", National Aerospace Laboratory NLR Report No. NLR-TP-2010-436, 2010.

[6] S. M. Spuler, D. Richter, M. P. Spowart and K. Rieken: "*Optical fiber-based laser remote sensor for airborne measurement of wind velocity and turbulence* ", Applied optics, 50 (6), 842-851, 2011.

[7] O. Kliebisch and P. Mahnke: "*Real-time laser Doppler anemometry for optical air data applications in low aerosol environments* ", Review of Scientific Instruments, 91 (9), 095106, 2020.

[8] T. Katsibas, T. Semertzidis, X. Lacondemine, and N. Grammalidis: "*Signal processing for a laser based air data system in commercial aircrafts*", 16th European Signal Processing Conference (Lausanne, Switzerland), 2008.

[9] C. M. Sonnenschein and F. A. Horrigan: "*Signal-to-Noise Relationships for Coaxial Systems that Heterodyne Backscatter from the Atmosphere*", Applied Optics, 10 (7), 1600-1604, 1971.

[10] Rod G. Frehlich and Michael J. Kavaya: "*Coherent laser radar performance for general atmospheric refractive turbulence*", Applied Optics, 30 (36), 5325-5352, 1991.

7. Glossary

ADC:	Analog-to-Digital converter
AoA/AOA:	Angle of attack
AOF:	Acousto-optic frequency shifter
AoS/AOS:	Angle of sideslip
BRAM:	Block random-access memory
CFD:	Computational fluid dynamics
DDRAM:	Double data rate random-access memory
DFB:	Distributed feedback
DMA:	Direct memory access
EMI:	Electromagnetic interference
FFT:	Fast Fourier transform
FL:	Flight level
IIO:	Industrial input/output
LDA:	Laser Doppler anemometer
LO:	Local oscillator
MOPA:	Master-oscillator power amplifier
PLL:	Phase-locked loop
TAS:	True air speed
TRA:	Temporary reserved airspace
TTOL:	Taxi, takeoff and landing